Tectonophysics 698 (2017) 109–120

Contents lists available at ScienceDirect

Tectonophysics

journal homepage: www.elsevier.com/locate/tecto

Controls on sill and dyke-sill hybrid geometry and propagation in the crust: The role of fracture toughness

J.L. Kavanagh [a,*], B.D. Rogers [a,b], D. Boutelier [c], A.R. Cruden [d]

[a] Department of Earth, Ocean and Ecological Sciences, University of Liverpool, Jane Herdman Building, 4 Brownlow Street, Liverpool L69 3GP, UK
[b] Department of Geosciences, Physics of Geological Processes, University of Oslo, Oslo, Norway
[c] School of Environmental and Life Science, University of Newcastle, Callaghan, NSW 2308, Australia
[d] School of Earth, Atmosphere and Environment, Monash University, Clayton Campus, Clayton, VIC 3800, Australia

ARTICLE INFO

Article history:
Received 17 May 2016
Received in revised form 5 December 2016
Accepted 26 December 2016
Available online 9 January 2017

Keywords:
Dyke
Sill
Analogue experiment
Gelatine
Fracture toughness
Magma intrusion

ABSTRACT

Analogue experiments using gelatine were carried out to investigate the role of the mechanical properties of rock layers and their bonded interfaces on the formation and propagation of magma-filled fractures in the crust. Water was injected at controlled flux through the base of a clear-Perspex tank into superposed and variably bonded layers of solidified gelatine. Experimental dykes and sills were formed, as well as dyke-sill hybrid structures where the ascending dyke crosses the interface between layers but also intrudes it to form a sill. Stress evolution in the gelatine was visualised using polarised light as the intrusions grew, and its evolving strain was measured using digital image correlation (DIC). During the formation of dyke-sill hybrids there are notable decreases in stress and strain near the dyke as sills form, which is attributed to a pressure decrease within the intrusive network. Additional fluid is extracted from the open dykes to help grow the sills, causing the dyke protrusion in the overlying layer to be almost completely drained. Scaling laws and the geometry of the propagating sill suggest sill growth into the interface was toughness-dominated rather than viscosity-dominated. We define K_{Ic}^* as the fracture toughness of the interface between layers relative to the lower gelatine layer K_{Iclnt} / K_{IcG}. Our results show that K_{Ic}^* influences the type of intrusion formed (dyke, sill or hybrid), and the magnitude of K_{Iclnt} impacted the growth rate of the sills. K_{Iclnt} was determined during setup of the experiment by controlling the temperature of the upper layer T_m when it was poured into place, with $T_m < 24$ °C resulting in an interface with relatively low fracture toughness that is favourable for sill or dyke-sill hybrid formation. The experiments help to explain the dominance of dykes and sills in the rock record, compared to intermediate hybrid structures.

1. Introduction

Constraining the physical processes that control magma transport through the lithosphere is fundamental in a wide range of geological contexts, from construction of the continental crust (e.g. Annen et al., 2006) to understanding the tendency and triggers of volcanic eruptions (Sigmundsson et al., 2010). Magma intrusion is much more frequent than magma eruption, with intrusion to extrusion ratios ranging from 5:1 in oceanic areas to 10:1 in continental areas (Crisp, 1984). At stratovolcanoes, it is estimated that only 10–20% of dykes reach the surface (Gudmundsson, 2002; Gudmundsson and Brenner, 2005). Whether magma intrudes the crust to form a magma chamber or transits directly to the surface to erupt will impact the style and frequency of global volcanism and therefore the associated hazards (e.g. Loughlin et al., 2015).

Intrusive magmatic bodies can form a variety of geometries across a wide range of scales: from dyke and sills, which are thin tabular magma intrusions that either cross-cut or intrude between crustal layers, respectively, to plutons that have lower aspect-ratio and are built through the accretion of smaller magma bodies (Glazner et al., 2004; Cruden and McCaffrey, 2001; Coleman et al., 2004). Magma ascends through the crust largely within fractures, interacting with crustal heterogeneities (e.g. stratigraphic layering, faults, joints, and lithological contacts). Crustal discontinuities may form a mechanical 'interface' between rock layers, and therefore a structural weakness that could be exploited by migrating magmas. The majority of magmatic intrusions do not culminate in surficial eruptions (Gudmundsson, 1983, 2002; Gudmundsson and Brenner, 2005); instead, many dykes go on to form sills at some critical point during their propagation (e.g. Magee et al., 2013). Dykes are often associated with extensional settings (e.g. Anderson, 1938) and some of the largest sills on Earth are found in rift-related sedimentary basins; they are important in the breakup of continents and the production of flood basalts (e.g. Muirhead et al., 2014). Sills can help to improve petroleum prospectivity (Malthe-Sørenssen et al., 2004; e.g. Gudmundsson and Løtveit, 2014), can be a host to diamondiferous kimberlite magma (Kavanagh and Sparks,

* Corresponding author.
E-mail address: janine.kavanagh@liverpool.ac.uk (J.L. Kavanagh).

http://dx.doi.org/10.1016/j.tecto.2016.12.027

2011; Gernon et al., 2012; White et al., 2012), and are an important resource in mineral exploration (e.g. REE, Ni, Cu, Mo, W, Sn, Au, Ag, Fe and platinum group elements (PGE); Barnes et al., 2016; Blundy et al., 2015; Naldrett, 2011).

Analogue modelling has proved to be an important tool in bridging the gap between field and monitoring data of magma intrusion processes, to test hypotheses and identify the key parameters that control magma ascent (see Rivalta et al. (2015) and Galland et al. (2015) for reviews). Recent progress has been made to quantify the mechanical properties of gelatine and its appropriateness as an analogue material to study magma intrusion in the crust (Kavanagh et al., 2013). In this paper, we present methods to measure the fracture toughness of elastic gelatine layers and the interface between layers, and use this to constrain the conditions leading to the formation of dykes, sills and hybrid geometries in nature. Detailed quantification of the evolving strain and stress in the elastic host material in the development of dyke-sill hybrid structures is presented using the photo-elastic properties of gelatine and digital image correlation (DIC) techniques. The importance of interfaces, as an example of a rock discontinuity, in the development of hybrid intrusions is discussed with implications for understanding magma ascent dynamics through the crust and the construction of large igneous bodies.

2. Theory and experimental framework

2.1. Hydraulic fractures

The theory of rock fracture mechanics is fundamental to magma intrusion in the crust. Dykes and sills can be considered as hydrofractures, i.e. rock fractures that are filled with, and formed by, a pressurised fluid (magma) (see Rivalta et al., 2015 for a comprehensive review). Theory states that the initiation of a hydrofracture occurs when the tensile strength of the host rock is exceeded by the overpressure P_0 of the intruding magma. If there is a density contrast ($\Delta\rho$) between the magma and the host then a buoyancy pressure P_b is generated across the vertical extent of the intrusion (h):

$$P_b = \Delta\rho g h. \quad (1)$$

For dyke ascent, it is not the density contrast along the entire dyke length but the 'local' buoyancy at the ascending head region that is important (referred to in the literature as the buoyancy length L_b, e.g. Taisne and Tait (2009) and Kavanagh et al. (2013)). An effective buoyancy contribution may come from a vertical gradient in stresses acting on the intrusion (Takada, 1989; Lister and Kerr, 1991), though for sill propagation this is likely to be minimal.

A hydrofracture will propagate if the mode I stress intensity factor K_I at the crack tip, which is a function of P_0 and the crack length L, exceeds a critical value known as the fracture toughness K_{Ic} of the host material. The overpressure of the magma must reach or exceed the fracture pressure P_f for the crack to grow:

$$P_0 > P_f = \frac{K_{Ic}}{\sqrt{L\pi}}. \quad (2)$$

Consequently, less overpressure is required for propagation as a crack grows in length.

In an isotropic material, the orientation and opening direction of a hydrofracture is determined by the principle stresses acting on the volume of material. The crack will open towards the minimum principal stress direction σ_3 with its length parallel to the maximum principal stress direction σ_1. In an anisotropic material, such as a rock with pre-existing fractures, then discontinuities may be intruded by magma if the overpressure exceeds the normal stress acting on them (Delaney et al., 1986).

2.2. Crust and magma analogue materials

Analogue experiments require the selection of carefully considered and appropriate materials to ensure that they are geometrically, kinematically and dynamically scaled with respect to nature (Hubbert, 1937). Finding analogue materials that are 'ideal' is, however, not straightforward; when studying dykes and sills the characteristics of both the host medium and the intruding fluid need to be considered, and experimental limitations and compromises commonly need to be made (Galland et al., 2015). Ideally the experiments should also allow the dynamics of intrusion to be easily measured, to record the evolution of the subsurface geometry and how it changes during growth.

In this study, pigskin gelatine was selected as the crust analogue material (Chanceaux and Menand, 2014; Daniels and Menand, 2015; Fiske and Jackson, 1972; Hyndman and Alt, 1987; Kavanagh et al., 2006, 2015; Menand and Tait, 2002; Rivalta et al., 2005; Taisne and Tait, 2011; Takada, 1990). Gelatine is a viscoelastic material, exhibiting viscous and elastic deformation in different proportions depending on concentration, temperature, age, strain or strain rate (Di Giuseppe et al., 2009; Kavanagh et al., 2013; van Otterloo and Cruden, 2016). At low temperature (5–10 °C), relatively short periods of time (tens of minutes) and for small applied stresses gelatine can be considered to be an almost ideal-elastic material. The mechanical properties of gelatine can be carefully controlled: its Young's modulus evolves with time and increases to a 'plateau' value, the magnitude of which is controlled by concentration and defines the time after which the gelatine can be considered 'cured'. Mixtures of between 2 and 5 wt% gelatine scale well to crustal rocks for experiments of magma intrusions in the crust (Kavanagh et al., 2013). Superposed layers of cured gelatine with well-constrained mechanical properties can be variably bonded, with either a strong or weak bond relative to the fracture toughness of the gelatine layers (see Kavanagh et al., 2015). Gelatine is a transparent substance, and as such the injection of fluid and growth of experimental intrusions can be observed in real time. Furthermore, it is photoelastic so the relative stresses revealed by birefringence colours can be observed using polarized light (e.g. Taisne and Tait, 2011).

Water is an appropriate analogue for magma in these experiments as it has low viscosity, and during injection it has low Reynolds number (Kavanagh et al., 2006). The density of water is also closely matched to gelatine, so buoyancy is negligible. Glycerine or glucose can be added to water to increase its density and viscosity, and the effects of solidification on intrusion dynamics can also be considered using temperature-dependent materials (e.g. Taisne and Tait, 2011; Chanceaux and Menand, 2014), but such variations are beyond the scope of this study.

2.3. Measurement and control of gelatine properties

2.3.1. Young's modulus E of gelatine layers

The Young's modulus of a gelatine layer was measured, when possible, immediately prior to an experiment being carried out by applying a load of known dimensions and mass to the free-surface and measuring the resulting deflection (Kavanagh et al., 2013):

$$E = \frac{mg(1-\nu^2)}{2ab}, \quad (3)$$

where m is the mass of the load, g is acceleration due to gravity, ν is Poisson's ratio (0.5 for gelatine), a is the radius of the load and b is the deflection of the top surface of the gelatine due to the load (see Kavanagh et al., 2013). Two loads were applied sequentially, and the average E reported (see Table 1 for load properties). Kavanagh et al. (2013) established that there is a linear relationship between gelatine concentration (wt%) and E, provided sufficient curing time has elapsed. In layered experiments, the Young's modulus of the lower layer E_1 and the rigidity ratio of upper layer relative to lower layer E_2 / E_1 cannot

Table 1
Properties of experimental loads used to calculate Young's modulus E, where 'm' is the mass of the load (kg) and 'a' is its radius (m). The averaged measurements of E are reported in Table 3.

	Geometry	*Material*	*m*	*a*
Load A	Cylinder	Brass	0.0501	0.0125
Load B	Cylinder	Brass	0.0418	0.0125

be measured directly and so these are estimated from concentration alone; however, the Young's modulus of the upper layer E_2 is measured.

2.3.2. Fracture toughness measurements K_{IcG} and K_{IcInt}

The fracture toughness K_{Ic} is a measure of a material's ability to resist fracture. The method to calculate K_{Ic} depends on the injection method of fluid into the gelatine layers, either a peristaltic pump at a constant volumetric flux (Q) (Kavanagh et al., 2015) or using a head pressure P_h (Kavanagh et al., 2013). The experiments we present here use a peristaltic pump to inject fluid into the gelatine solids.

The elastic pressure P_e (Lister and Kerr, 1991), equivalent to the overpressure P_0, required to open the fluid-filled fracture is calculated as follows:

$$P_e = \frac{E}{2(1-\nu^2)}\frac{H}{L} \tag{4}$$

where H is the thickness and L is the length of the fluid-filled fracture. When a peristaltic pump injects the fluid, K_{Ic} of the gelatine layers and interface can be calculated provided it can be demonstrated that the fracture pressure (Eq. (2)) and elastic pressure (Eq. (4)) are in equilibrium $P_f = P_e$ (Kavanagh et al., 2015):

$$K_{Ic} = \frac{EH\sqrt{\pi}}{2(1-\nu^2)\sqrt{L}}. \tag{5}$$

The volumetric flux Q is measured as the volume of outflow from the injector per second.

2.3.3. Interface fracture toughness control: gelatine mixture temperature T_m

During preparation of the experiment, the temperature T_m of the upper gelatine layer is recorded when it is poured onto the solidified lower layer. The temperature of the lower layer was ~5 °C when the upper layer was poured into place. Previous work suggests that the mechanical properties of the interface between the gelatine layers is controlled during experiment preparation by varying the temperature contrast between the lower cold, solid gelatine layer and the new hot gelatine layer when it is emplaced (Kavanagh et al., 2006, 2015). It has been suggested that a 'strong' interface is produced if the upper layer is poured into place at a temperature that is several degrees higher than the gelling temperature of the lower layer (T_{gel} ~ 20 °C), due to it temporarily melting the lower layer and welding to it. In contrast, when layer 2 is emplaced at a temperature close to T_{gel} a 'weak' interface is produced as minimal melting of the lower layer occurs.

3. Methodology

3.1. Experiment preparation and setup

Preparation of the gelatine analogue experiments involves production of mixtures of specified concentration (X wt%) and temperature (T_m °C). The gelatine was prepared by dissolving a measured quantity of pig-skin gelatine powder (260 bloom, 20 mesh, from Gelita UK) in hot distilled water (~90 °C) to a specified concentration (see Table 2). The majority of the experiments had the same gelatine concentration for layer 1 and layer 2 (2.5 wt%), though one experiment had a slightly more concentrated upper layer (MOPIV6 layer 2: 3.0 wt%). The hot gelatine mixture was then poured into a clear-Perspex tank, and all bubbles were removed from the surface. Two types of clear-Perspex container were used (see Fig. 1), either a 'large' square-based tank (measuring $40 \times 40 \times 30$ cm^3) or a 'small' cylindrical tank (15 cm diameter and 20 cm height). To inhibit the collection of any condensation that might be formed onto the gelatine surface during the cooling process, some experiments had oil poured onto the liquid gelatine prior to it being put into a refrigerator at 5 °C to cool. This oil was then completely removed prior to layer 2 being emplaced. Otherwise, the container was covered with plastic film and the tank moved to the refrigerator. Both methods inhibited the development of a rigid 'skin' on the gelatine surface and so ensured each layer's mechanical homogeneity. Once layer 1 had 'gelled' the next layer was prepared using the same method. Experiments were performed by injecting dyed water into the base of the tank via a tapered-injector using a peristaltic pump (controlled volumetric flux; Fig. 1). Rheometer data presented in Kavanagh et al. (2015) suggests that gelatine solids behave elastically at these experimental conditions. The initial stress conditions were hydrostatic and experimental variables included the size of container, rigidity contrast (E_2 / E_1) and T_m (see Tables 2 and 3). High-definition video cameras placed around the experimental tank recorded the growth of the resulting experimental intrusions.

Table 2
Parameters, variables and intrusions forms of the 'large' and 'small' tank experiments. X (wt%) = gelatine concentration, M (kg) = mass of gelatine-water mixture used in each layer, D (cm) = thickness of gelatine layer, T_s (°C) = temperature of solid gelatine layer 1 immediately prior to pouring layer 2 in place during experiment preparation, T_m (°C) = mixture temperature of layer 2 gelatine when poured on to cooled layer 1, '*Int type*' refers to the method used to prepare the interface between gelatine layers where C = cling-wrap and O = oiled, T (°C) = temperature of gelatine solids at time of running the experiment, t (hours) = amount of time gelatine has been curing in the refrigerator (layer 2, where layer 1 has cured for ~24 h longer), and Q ($\times 10^{-7}$ m^3/s) volumetric flow rate (flux) of injected fluid. Subscripts *1* and *2* refer to the lower and upper gelatine layers, respectively.

	X_1	X_2	M_1	M_2	D_1	D_2	T_s	T_m	*Int type*	T	t	Q	*Intrusion formed*
Large tank experiments													
LBR2	2.5	2.5	20	20	11.2	12.6	5	21.3	O	7.5	116	3.9	Dyke-sill hybrid
LBR4	2.5	2.5	20	20	11.4	12.4	5	20.3	C	6.8	124	3.9	Sill
LBR5	2.5	2.5	20	20	11.4	12.9	5	19.4	C	6.9	167	3.9	Sill
LBR6	2.5	2.5	20	20	11.5	12.2	5	20.0	C	6.8	168	3.9	Dyke-sill hybrid
MOPIV6	2.5	3	20	20	12.2	12.4	5	22.0	C	7.6	67	3.9	Dyke-sill hybrid
MOPIV9	2.5	2.5	20	20	12.5	12.5	5	21.0	C	6.7	66	3.9	Sill
Small tank experiments													
SBR17	2.5	2.5	3	2	10.6	7.2	5	22.3	C	6.9	121	3.9	Dyke-sill hybrid
SBR18	2.5	2.5	3	2	10.3	7.7	5	24.2	C	6.1	121	3.9	Dyke erupted
SBR19	2.5	2.5	3	2	10.7	7.3	5	22.0	C	6.0	121	3.9	Sill
SBR20	2.5	2.5	3	2	10.6	7.8	5	23.0	C	6.4	122	3.9	Sill
SBR21	2.5	2.5	3	2	10.7	7.7	5	21.7	C	6.6	122	3.9	Dyke-sill hybrid

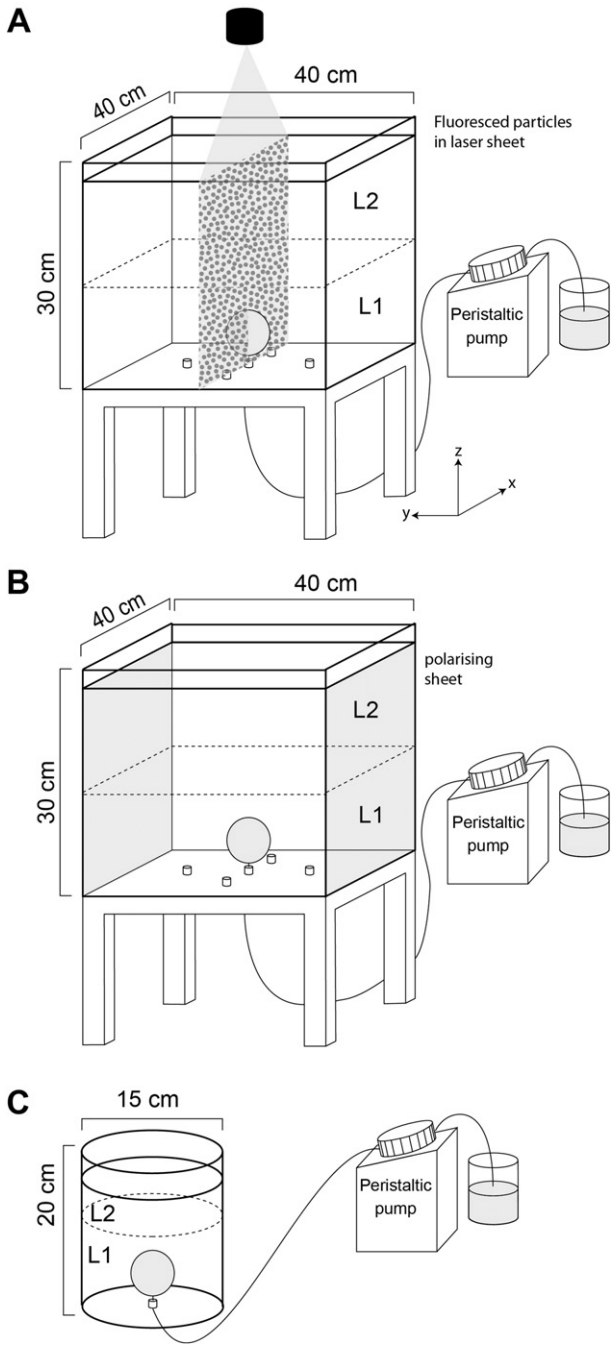

Fig. 1. Schematic illustration of experiment apparatus and setup of two-layered gelatine experiments injected with water by a peristalic pump. A) Neutrally-buoyant particles were added to the gelatine during its preparation; these fluoresced when intersected by an overhead thin, vertical laser sheet oriented parallel to the feeder dyke's thickness during the experiment. B) Polarised sheets were fitted to the exterior of the tank, the gelatine's photoelasticity produced colour fringes of stress concentration during fluid injection. The clear-Perspex experiment containers were 'large' 30 cm high and 40 cm square (A, B), or 'small' 15 cm diameter cylinders (C).

3.2. Mapping stress and strain evolution in gelatine: Photoelasticity and digital image correlation (DIC)

A set of polarizing plates were attached to the outside of the tank to utilise the photoelasticity of gelatine and visualise stress changes in the gelatine host as it was injected by water. Experiments were viewed with polarised light (Fig. 1B) where colour fringes indicate qualitative stress perturbations (e.g. Taisne and Tait, 2011).

Table 3
Results from experiments where fluid was injected at a constant volumetric flow rate (flux). E (Pa) = Young's modulus (±10%; average measurement recorded, using two different experimental loads (Table 1)), E_2 / E_1 = model ratio of Layer 2 and Layer 1 Young's moduli assuming gelatine has cured (see Kavanagh et al., 2013), K_{Ic} (Pa $m^{0.5}$) = fracture toughness calculated assuming pressure equilibrium. Subscripts *1* and *2* refer to the lower and upper gelatine layers, respectively, '*G*' refers to a gelatine layer 1 and '*int*' refers to the interface. $K_{Ic}{}^{*} = K_{Iclnt}$ / average K_{IcG} (average K_{IcG} = 103 Pa $m^{0.5}$ (large tank) or 106 Pa $m^{0.5}$ (small tank) for sill or dyke-sill hybrid-forming experiments where $E_2 = E_1$). As SBR21 did not meet the pressure-equilibrium criteria, its K_{IcG} and K_{Iclnt} could not be calculated. ^Estimated value as K_{Iclnt} could not be measured in this dyke-forming experiment.

	E_2	E_2 / E_1	K_{IcG}	K_{Iclnt}	$K_{Ic}{}^{*}$
LBR2	6201	1	116	69	0.66
LBR4	5758	1	89	53	0.51
LBR5	5546	1	103	33	0.32
LBR6	5885	1	109	56	0.54
MOPIV6	7740	1.42	67	23	0.22
MOPIV9	5170	1	100	45	0.43
SBR17	6527	1	90	68	0.65
SBR18	5922	1	83	–	1.00^
SBR19	7076	1	107	62	0.59
SBR20	8204	1	122	50	0.48
SBR21	8777	1	–	–	–

Strain evolution was measured quantitatively in the experiments using digital image correlation (DIC) techniques (e.g. Kavanagh et al., 2015). In the experiments presented here, a frequency doubled Nd:YAG laser sheet was triggered from above, illuminating fluorescent seeding particles (PMMA-RhB, 20–50 μm, density 0.98 g/cc) added to the gelatine during its preparation (see Fig. 1A and Kavanagh et al. (2015)). The thin laser sheet (approximately 1 mm thick) illuminated a vertical 2-dimensional xz-plane through the experiment, and intersected the centre of the tank (the point of injection). A CCD camera (LaVision Imager Pro X 4M, 2048 × 2048 pixel resolution) recorded images of the fluoresced particles, synchronised with each laser pulse. Images were recorded at 2 Hz for up to 60 min. A 532–546 nm pass band filter in front of the camera lens was used to eliminate stray reflections of laser light.

Processing of the laser-fluoresced images was carried out using LaVision DaVis 8 software. The field of view analysed was 40 × 30 cm^2 and the image resolution was approximately 5 pixels/mm. The recorded images were sub-sampled to 5-second intervals, and cross-correlation between successive images 'pattern matched' the fluoresced passive tracer particles to calculate displacement vectors within the gelatine. The analysis window-size was 64 × 64 pixels with an overlap of 87%, and a multi-pass filter with decreasing window size allowed high precision (sub-pixel) and high resolution measurements of the incremental and cumulative displacements to be calculated (e.g. Adam et al., 2005; Schrank et al., 2008; Kavanagh et al., 2015). When gelatine deforms elastically the measured strain correlates with stress, and this relationship can be quantified using rheometric data (Kavanagh et al., 2015).

4. Results

In total 11 experiments were carried out (Table 2), primarily varying the size of the experiment (large or small tank), the temperature at which layer 2 was emplaced (T_m), and the concentration of the gelatine layers (subscripts 1 and 2 refer to the lower and upper layers, respectively). The layer thickness (D_1 and D_2), layer 2 curing time (t), gelatine temperature at the time the experiment was run (T) and interface type (oiled or cling-wrap) was also recorded. The Young's modulus of the gelatine was measured to be ~5000–8800 Pa, which scales to ~0.3–4.4 GPa in nature (Kavanagh et al., 2013); this value is comparable to typical sedimentary rock layers, but is towards the lower end of values anticipated for sedimentary rocks at depth.

A range of sheet-intrusion geometries were produced in the experiments, including dykes, sills, and dyke-sill hybrids (Table 2). Sills were formed when the ascending dyke quickly turned to form a sill when

reaching the interface. Erupted dyke fissures occurred when the ascending dyke cut across the interface between the layers and ascended to erupt at the surface. Intermediate dyke-sill hybrid structures occurred when the ascending dyke crossed the interface but also intruded it; in these cases the dyke protrusion that crossed the interface did not go on to erupt. Similar structures have been produced in previous studies (e.g. Kavanagh et al., 2006, 2015), but in Section 4.1 we focus on the formation of the less studied and relatively poorly understood dyke-sill hybrids.

4.1. Mechanics of dyke-sill hybrid intrusion formation and growth

Dyke-sill hybrid intrusions were produced five times in the experiments. Fig. 2 shows a series of photographs of an experiment where a dyke-sill hybrid formed (LBR2). The vertical penny-shaped dyke intrusion first penetrated through the lower gelatine layer and then into the upper gelatine layer, and very shortly afterwards intruded the interface forming two distinct sills at the dyke's lateral tips (Fig. 2A). The two sills grew quickly as they spread out into the interface between the gelatine layers (Fig. 2B). The sills subsequently merged together and joined the dyke margins at the interface to create the full hybrid structure (Fig. 2C).

Fig. 3 (see also Supplementary Video Fig. 3) shows a hybrid intrusion growth viewed with polarised light, illustrating qualitative stress perturbations in the gelatine by the development and movement of colour fringes. As the dyke ascended through the lower gelatine layer stresses were concentrated at the head region, displaying the typical "bow tie" stress distribution expected during crack tip propagation in an elastic material (e.g. Pollard and Johnson, 1973). Stresses then accumulated along the entire interface plane as it was approached by the intrusion. When the dyke crossed the interface, stress remained concentrated at the dyke tip as it protruded into layer 2. Shortly afterwards a sill formed by intruding the interface, and stresses were then concentrated at the growing sill margin. As the sill grew, stresses appear to be gradually reduced around the dyke protrusion in layer 2 but are difficult to see in layer 1.

Digital image correlation (DIC) was carried out to quantify strain changes in the gelatine as a dyke-sill hybrid intrusion was formed. During injection of the fluid, measurements were made within a 2-dimensional vertical plane through the gelatine solid that was illuminated by the laser sheet oriented perpendicular to the strike-direction of the feeder dyke. Fig. 4 (see also Supplementary Video Fig. 4) is a compilation of frames recorded during a dyke-sill hybrid experiment (MOPIV6) and is the 'raw' data used in the DIC analysis. Fig. 5 (see also Supplementary Video Fig. 5) presents the processed data, plotting horizontal incremental strain (elongation) ε_{xx} calculated at 5-second intervals within the plane of the laser sheet. Key time intervals of significant changes in ε_{xx} during dyke-sill hybrid formation are shown in Fig. 5A–F. During the initial ascent of the dyke through gelatine layer 1, incremental strain accumulated at the small tip-region of the dyke, and displacement vectors indicate progressive opening of the fluid-filled crack; at 25–30 s after the start of injection ε_{xx} had a maximum value of 23 % (Fig. 5A). The dyke reached the interface between the gelatine layers at 145–150 s; at this time ε_{xx} had reduced to a maximum value of 1.7 % and strain was more distributed along the length of the dyke (Fig. 5B). At this time a small amount of strain had also accumulated within gelatine layer 2 directly above the dyke. Subsequently the dyke propagated across the interface into layer 2 at 315–320 s, with strain continuing to be concentrated in a small tip-region but with a slightly increased maximum ε_{xx} ~ 2.3% (Fig. 5C). Sill formation occurred at 330–335 s and it was followed by a rapid decrease in horizontal incremental strain in the gelatine around the feeder dyke, shown by negative ε_{xx} values (Fig. 5D). However, incremental strain continued to accumulate simultaneously in the dyke protrusion in layer 2, with maximum values of 1.7 %. As sill propagation continued, the feeder dyke in layer 1 continued to contract and was associated with increasingly negative incremental strains in the adjacent gelatine (ε_{xx} reduced to −3.0 %) with a small amount of positive strain remaining at the dyke tip in layer 2 (Fig. 5E). The final stages of sill growth caused the dyke protrusion in layer 2 to also contract, with negative incremental strains distributed along the entire dyke (at 340–345 s, Fig. 5F).

To determine the evolution of total strain e_{xx} during dyke-sill hybrid formation an experiment was analysed using DIC in a 5 mm x 5 mm square area adjacent to the centre of the feeder dyke in the lower layer (MOPIV6). In Fig. 6, the results from this analysis are compared with MOPIV9 which is a sill-formation example from Kavanagh et al. (2015) (there called Exp 5). The Kavanagh et al. (2015) experiment was prepared in the same way as MOPIV6, has the same injection flux and a weak interface but $E_2 = E_1$. The two experiments showed similar

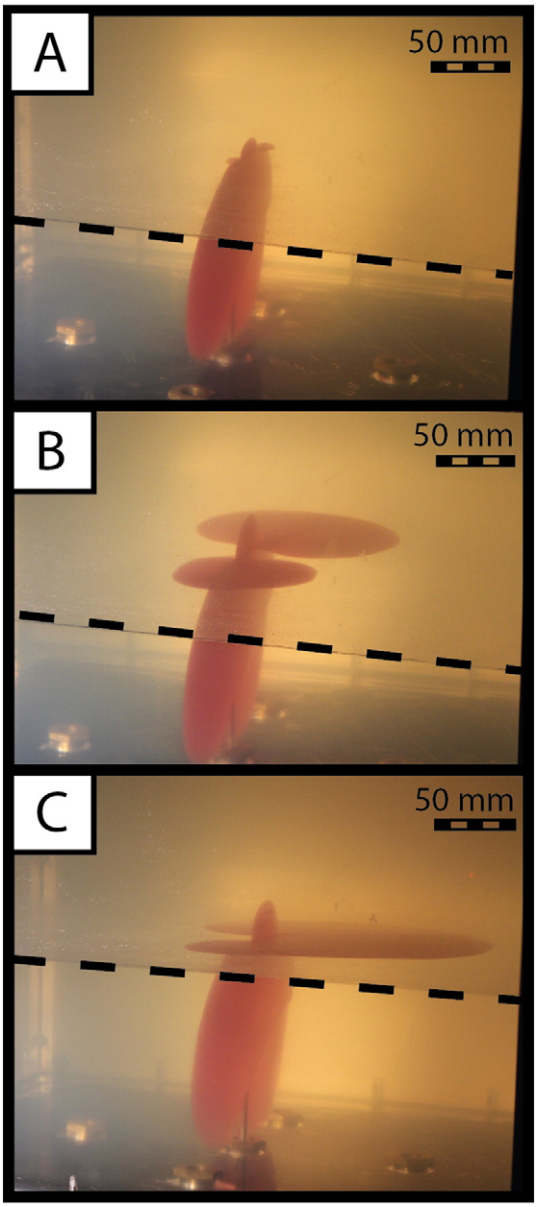

Fig. 2. Dyke-sill hybrid formation (LBR2) in one of the 'large' tank experiments. The intrusion is viewed looking down and from the side, onto the interface between the gelatine layers. The position of the interface against the tank wall is indicated by the dashed line. A) A penny-shaped dyke has propagated through the lower gelatine layer and slightly protruded into the upper layer, with two small sills intruding the horizontal interface where it is intercepted by the dyke margins. B) The dyke protrusion in the upper layer quickly became arrested as the sills grew. C) The sills joined together within the interface, continued to grow and then coalesced with one margin of the dyke to create the final dyke-sill hybrid structure.

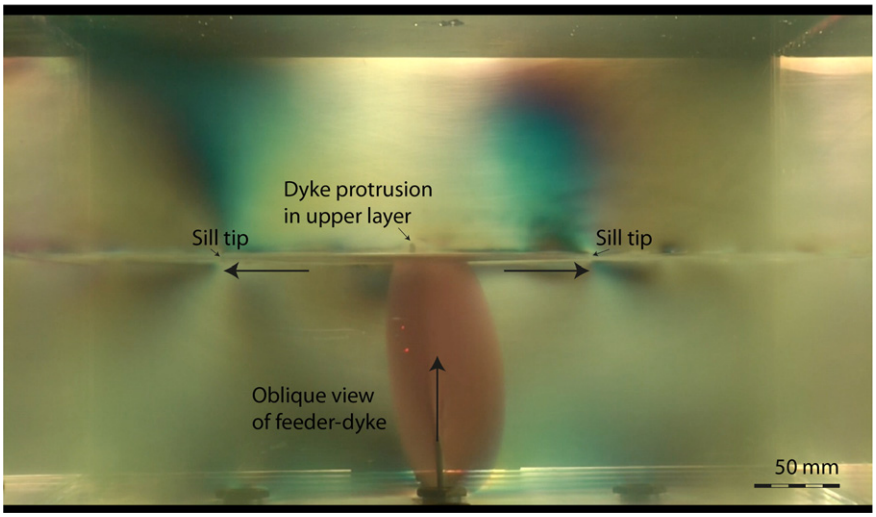

Fig. 3. Video of dyke-sill hybrid formation (experiment LBR6). The intrusion is viewed with polarised light, approximately perpendicular to the strike direction of the dyke. Interference colours indicate the evolving distribution and intensity of stress within the gelatine host.

evolution in e_{xx} with four phases of intrusion growth identified. In both experiments, the area monitored experienced a gradual increase in total strain as the dyke propagated towards and then beyond it. Secondly, in both experiments sill formation caused a rapid contraction of the feeder dyke and a rapid decrease in e_{xx}. Thirdly, as the sills grew their feeder dykes continued to contract and total strain continued to decrease. At the moment the injection pump was turned off there was a small and rapid additional decrease in e_{xx} detected in both experiments. However, with a maximum total strain of ~35% compared to ~50%, the dyke-sill hybrid-forming experiment reached a lower maximum total strain that the sill-forming experiment. The moment of sill formation occurred simultaneously in the two experiments and the rate of decrease in e_{xx} was identical, but overall the accompanying rapid decrease in total strain at sill formation was greater in magnitude in the sill-forming experiment at 33% (50% down to 17%) compared to 15% (35% down to 20%) in the dyke-sill hybrid experiment.

4.2. Toughness-dominated or viscosity-dominated propagation?

There is some discussion in the literature regarding the nature of sill propagation dynamics, when intrusion occurs into a weak boundary (or interface) between elastic layers. For dykes it has been established in gelatine-based analogue experiments that propagation occurs in the fracture toughness-dominated regime such that $P_0 \sim P_f$ (e.g. Menand and Tait, 2002). However, some studies have suggested that sill propagation dynamics could be viscosity-dominated such that instead $P_0 \sim P_v$, where P_v is the viscous pressure (e.g. Kavanagh et al., 2006; Chanceaux and Menand, 2016).

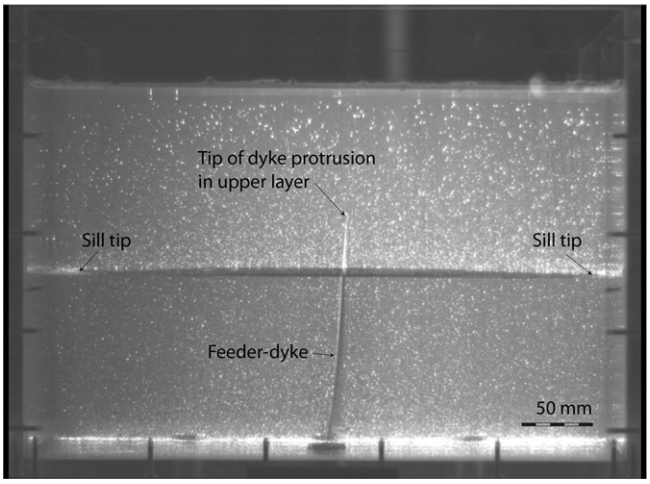

Fig. 4. Dyke-sill hybrid formation, with fluorescent particles in the gelatine illuminated by a thin vertical laser sheet (experiment MOPIV6). Video complied from successive images collected with a CCD camera. The intrusion is viewed perpendicular to the dyke strike direction.

4.2.1. Equilibrium length and thickness ratios

It has been demonstrated in previous studies that the expected length and thickness of a pressurized fluid-filled crack intruding an elastic material can be calculated assuming a pressure equilibrium that is either fracture toughness- or viscosity- dominated. The toughness equilibrium model assumes the fracture pressure P_f (Eq. (2)) and elastic pressure P_e (Eq. (4)) are equal for a given injection flux (for details see Appendix of Kavanagh et al., 2015), and from this K_{Ic} can be calculated (Eq. (5)). Instead, the viscosity equilibrium model assumes that the elastic pressure P_e is equal to the viscous pressure P_v for a given injection flux (Chanceaux and Menand, 2016):

$$P_v = \frac{12\mu L^2}{H^2 t} \tag{6}$$

where μ is the viscosity of the intruding fluid, H is the thickness and L the length of the intrusion at time t after sill injection.

Fig. 7 plots dyke length against time for several experiments where fluid was injected with constant flux in a large tank (A) and small tank (B). The toughness equilibrium model is shown and defines the expected change in the length of the dyke (±10%). Fig. 7A shows that in the large-tank experiments the length evolution of the dykes in layer 1 indicates they all formed in toughness-dominated pressure-equilibrium as they fall within 10% error of the model. Fig. 7B shows that all small tank experiments except SBR21 can also be considered to have formed in equilibrium within error, although the fit of the data to the model curves is not as good in the small tanks compared to the large tank experiments. These results suggest that dyke propagation in our experiments occurred in the toughness-dominated regime.

Fig. 8 plots sill length, thickness and length/thickness ratio of a representative sill-forming experiment MOPIV9, where the intrusion was imaged using a laser sheet positioned through the centre of the intrusion and so the geometry measurements have a small error. Model length, thickness and their ratio over time are plotted assuming propagation was toughness- or viscous- dominated. Fig. 8A shows the experimental sill length lies almost equally between that modelled by the two

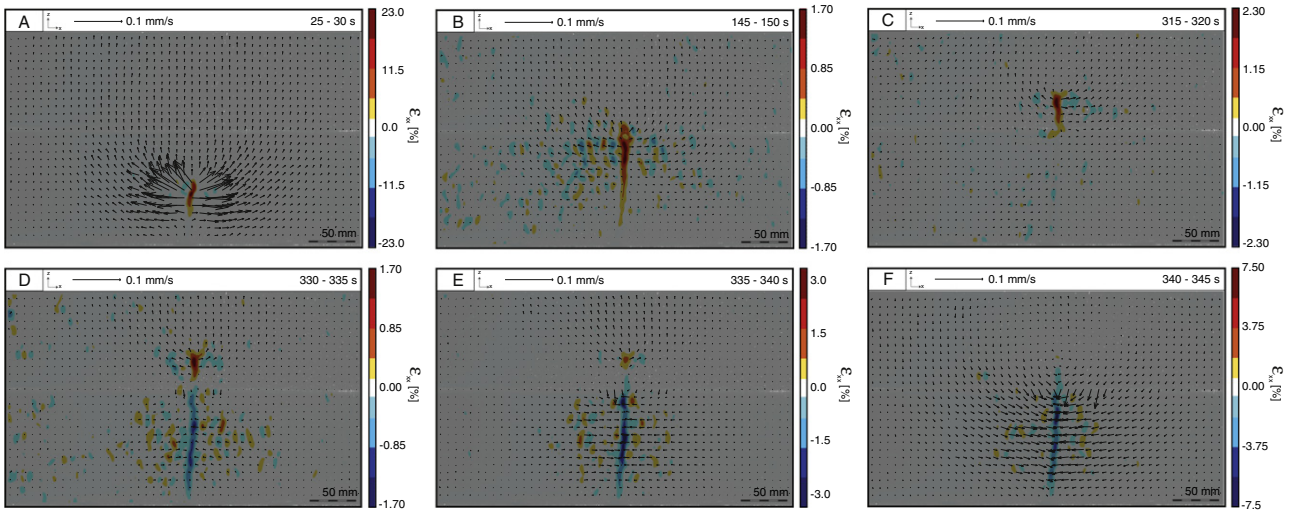

Fig. 5. Video showing digital image correlation (DIC) model of dyke-sill hybrid formation (MOPIV6), plotting incremental strain ε_{xx} (at 5-second intervals). Selected time frames of incremental strain evolution in the gelatine host during dyke-sill hybrid formation are shown in A–F. The black vector arrows indicate the direction and magnitude of gelatine displacement, and the colour-map indicates the calculated incremental strain (ε_{xx} %). The experimental intrusion is viewed perpendicular to the dyke strike direction. A) 25–30 s, B) 145–150 s, C) 315–320 s, D) 330–335 s, E) 335–340 s, and F) 340–345 s.

regimes, being initially quite close to the viscous-dominated model but moving progressively towards the toughness-dominated expected length with time. However, the graphs of sill thickness (Fig. 8B) and the length/thickness ratio (Fig. 8C) show these are consistently closer to that expected by the toughness-dominated model throughout the sill growth. It is clear that the dynamics of sill propagation in our experiments are complex, however the results indicate that they are overall better described by the toughness-dominated model.

4.2.2. Fracture toughness calculations K_{IcG} and K_{IcInt} and relationship with T_m

Given that Figs. 7 and 8 indicates that it is valid to assume $P_e \sim P_f$ for both dyke and sill propagation in several of the analogue experiments, and therefore that propagation was overall toughness-dominated, we conclude that it is appropriate to use Eq. (5) to calculate the fracture toughness of the lower gelatine layer (K_{IcG}) and the interface between gelatine layers (K_{IcInt}). The results of these calculations are shown in Table 3 and use the Young's modulus of the upper layer E_2 as well as the length and thickness measurements of the dyke taken immediately prior to sill formation for K_{IcG} and immediately after sill inception for K_{IcInt}.

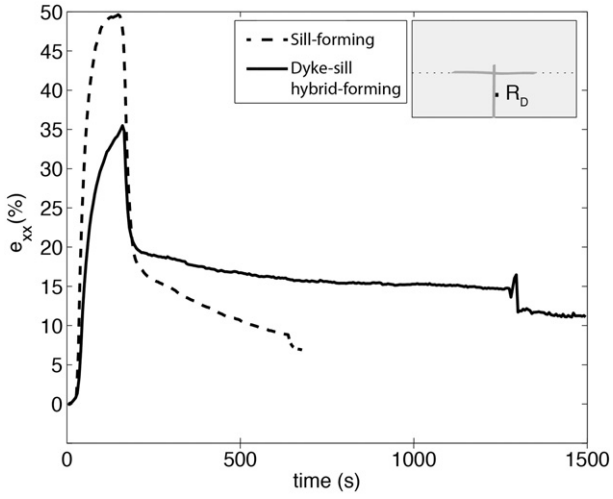

Fig. 6. Evolution of finite strain (e_{xx} %) in a 5 mm × 5 mm area (indicated in panel inset) adjacent to the feeder dyke of a dyke-sill hybrid experiment (MOPIV6) and a sill-forming experiment (MOPIV9). In both experiments at the moment of sill formation and feeder dyke contraction (160–165 s) there was a rapid decrease in e_{xx}, though this decrease was greater in the sill-forming experiment than the dyke-sill hybrid one.

In most cases it has been possible to calculate K_{IcG}, however it is only experiments which were sill-forming or dyke-sill hybrid-forming that it has been possible to calculate K_{IcInt}. Where it was possible to calculate K_{IcG} the average was found to be 102 Pa $m^{0.5}$, which is consistent with previously published values of 2.5 wt% gelatine solids tested at comparable experimental conditions (Kavanagh et al., 2013, 2015). The mean K_{IcG} was slightly smaller for the large tank experiments at 103 Pa $m^{0.5}$ compared to the small tank experiments at 106 Pa $m^{0.5}$ (when dyke-sill hybrids or sills were formed and $E_2 = E_1$). We note that an alternative equation to calculate fracture toughness of gelatine solids $K_{Ic} = 1.4(\pm 0.1)\sqrt{E}$, proposed by Kavanagh et al. (2013), produces very similar values; calculations using an estimated E, based on the assumption layer 1 has cured, rather than measured E_2 give similar but slightly higher values of K_{IcG}. In comparison, the mean fracture toughness of the interface K_{IcInt} was calculated as 52 Pa $m^{0.5}$ with a median of 55 Pa $m^{0.5}$, and it was always less than K_{IcG}.

K_{IcG} and K_{IcInt} of large-tank experiments that formed sills or dyke-sill hybrids are plotted against T_m in Fig. 9. The results show that K_{IcInt} is positively correlated with T_m (coefficient of determination $r^2 = 0.48$) following the empirical relationship:

$$K_{IcInt} = 12.1T_m - 197. \quad (7)$$

This suggests that K_{IcInt} can be calculated experimentally based purely on measurement of T_m. The intersection of the K_{IcInt} model with the mean K_{IcG} identifies an upper bound for K_{IcInt} that can be achieved in the experiments when T_m is between 24 and 25 °C (for a 2.5wt concentrated gelatin at 5 °C).

4.2.3. Fracture toughness ratio impact on intrusion geometry

To explore the parameter space further, we introduce the normalized fracture toughness $K_{Ic}^* = K_{IcInt} / K_{IcG}$ and plot this against T_m and according to the type of intrusion formed (Fig. 10). Two distinct fields are evident in Fig. 10: 1) a dyke-forming region where $K_{Ic}^* \geq 1$ and $T_m > 24$ °C, and 2) a sill-forming or dyke-sill hybrid-forming field where $K_{Ic}^* < 1$, where lower K_{Ic}^* values tend to be associated with sill formation. Calculated values of K_{Ic}^* are shown in Table 3. An estimated value of 1 was assigned to dyke-forming experiment SBR18, as the interface was not intruded its fracture toughness could not be measured

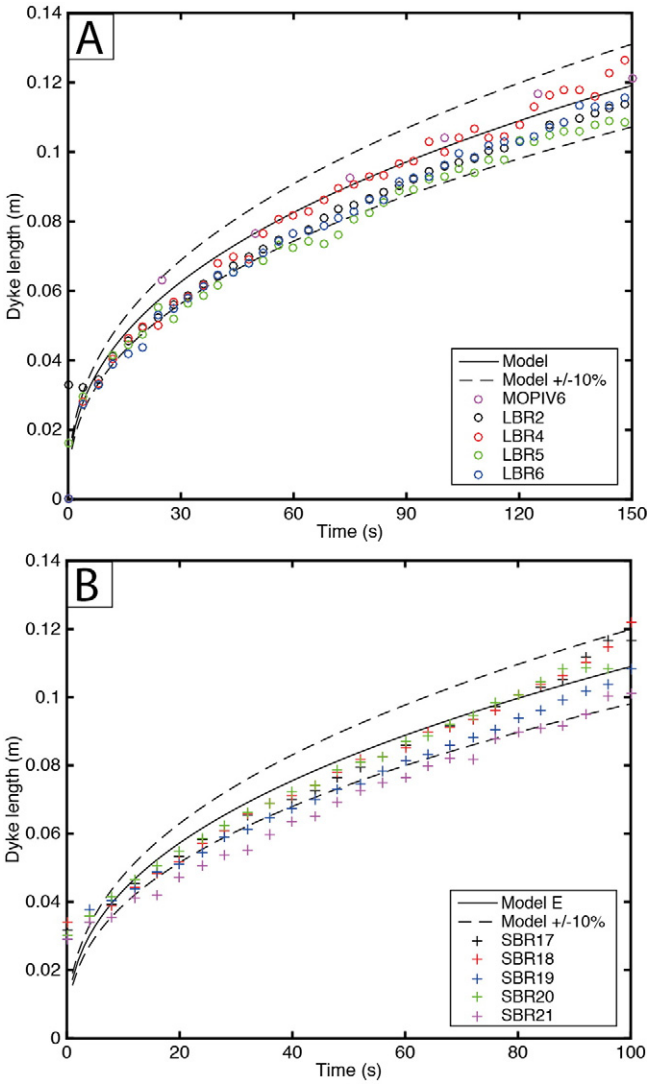

Fig. 7. Dyke length ±0.002 m, approximately the length of the symbol) versus time in large and small tank experiments. The model (solid-line) defines the geometry expected if the injections are in fracture toughness pressure equilibrium (±10% uncertainty, dashed-lines). A) Large tank experiments, Young's modulus E = 5850 Pa and fracture toughness K_{IcG} = 104 Pa $m^{0.5}$, B) small tank experiments E = 7300 Pa and K_{IcG} = 108 Pa $m^{0.5}$. In both cases the models assume constant flux Q = 3.9×10^{-7} m^3/s. Most of the experimental measurements lie within the dashed lines and so indicate the assumption of equilibrium is valid, excluding SBR21.

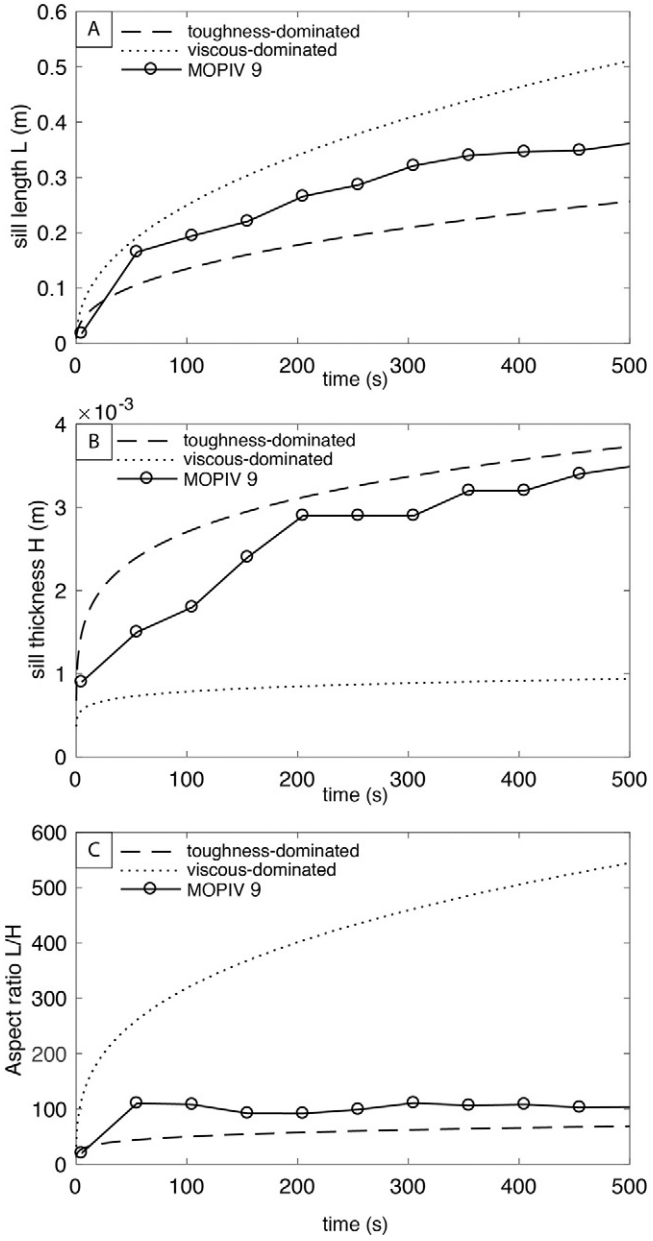

Fig. 8. Sill length (A), thickness (B) and aspect ratio (C) (solid line, ±0.002 m) versus time for experiment MOPIV9. Two equilibrium models are shown which define the sill geometry expected if the injections are in a toughness-dominated regime (dashed line) or viscosity-dominated regime (dotted line). E = 5170 Pa, K_{Iclnt} = 45 Pa $m^{0.5}$, Q = 3.9×10^{-7} m^3/s and μ = 8.9×10^{-7} Pa s.

directly. Potentially the conditions where $K_{Ic}^* > 1$ could be explored experimentally if the upper layer were stiffer than the lower layer and the interface was not intruded. However, experiment MOPIV6 which had $E_2 > E_1$ was dyke-sill hybrid-forming and had $K_{Ic}^* < 1$ (Table 3). In none of our experiments did we measure or infer $K_{Ic}^* > 1$, however fracture toughness tests on rock interfaces have suggested this could be realised in nature (Kavanagh and Pavier, 2014) so would be interesting to explore in future experiments.

Fracture toughness of the gelatine layers and their interface not only influenced the geometry of intrusions that were formed, but also the propagation dynamics of the sill growth. This is shown in Fig. 11 where the change in length of sill is plotted against time for two sill experiments (LBR4 and LBR5) and a dyke-sill hybrid experiment (LBR6). In all three experiments there is an initial stage of rapid sill growth for up to ~40 s, and then a second phase of slower growth until the sill reached the tank wall. Sill growth was asymmetrical and predominantly towards one tank wall. During the initial stages of sill formation, faster growth rates were associated with interfaces that had lower fracture toughness (Fig. 10). The mechanical properties of the interface have therefore not just determined the type of intrusion formed (sill, hybrid, or dyke) but has also affected the growth dynamics of the sill as the interface is intruded. A change in sill growth rate was indicated by the change of slope on the distance-time plot; this may be due to interaction with the tank walls, or instead marks the time when the sill began to strongly interact with the free surface as its length became greater than the layer thickness (D_2) (see Bunger and Cruden, 2011).

4.3. Scaling laws of toughness- or viscosity- dominated regimes

The existence of viscosity-dominated and toughness-dominated regimes for penny-shaped sills is well established in the mechanics and hydrofracture literature. To further explore the nature of sill propagation in our experiments we apply the model of Savitski and Detournay

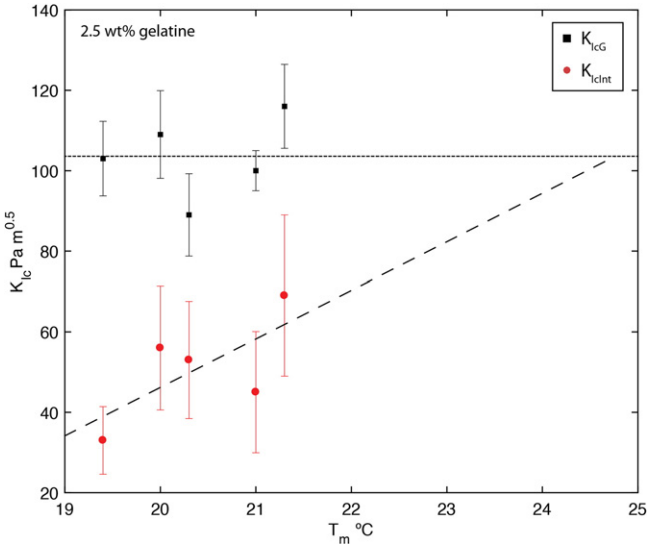

Fig. 9. Fracture toughness of the upper gelatine layer K_{IcG} and interface fracture toughness K_{IcInt} plotted against T_m (the preparation temperature of the upper layer when poured in place). Average K_{IcG} is indicated as 103 Pa m$^{0.5}$. T_m and K_{Ic} of the interface are positively correlated, and the dashed-line shows the line of best fit $K_{IcInt} = 12.1*T_m$-197 (R^2 = 0.48). Only the results from large tank experiments are shown; $X_1 = X_2 = 2.5$ wt%, and $E_2 = E_1$.

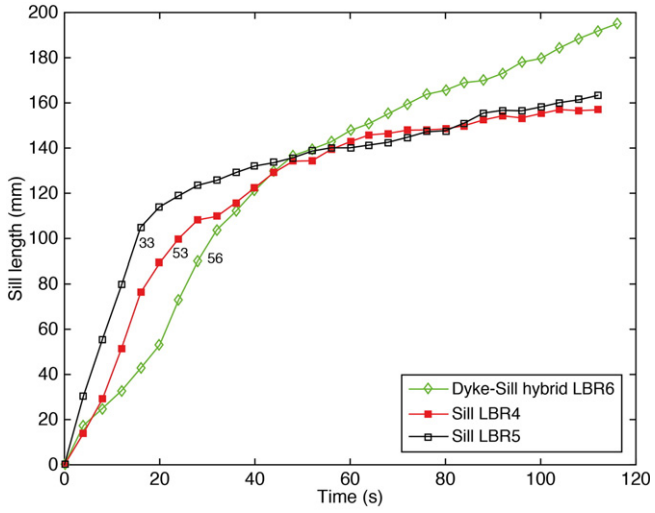

Fig. 11. Sill length (±2 mm, ~ symbol size) versus time (s) since sill inception in three large-tank experiments that are sill-forming (squares, LBR4 and LBR5) and dyke-sill hybrid-forming (diamonds, LBR6). The calculated fracture toughness of the interface K_{IcInt} intruded by the sill is indicated, showing that sills grew faster when the interface fracture toughness was lower.

(2002) who examine a penny-shaped hydrofracture propagating in an infinite elastic region. This model is similar in approach to Bunger and Cruden (2011), who study the emplacement of shallow sills under a thin, plate-like overburden, and is equivalent to comparing pressure scales to calculate when during intrusion growth the dynamics are viscosity- or toughness-dominated.

Savitski and Detournay (2002) define three parameters:

$$\mu' = 12\mu \tag{8}$$

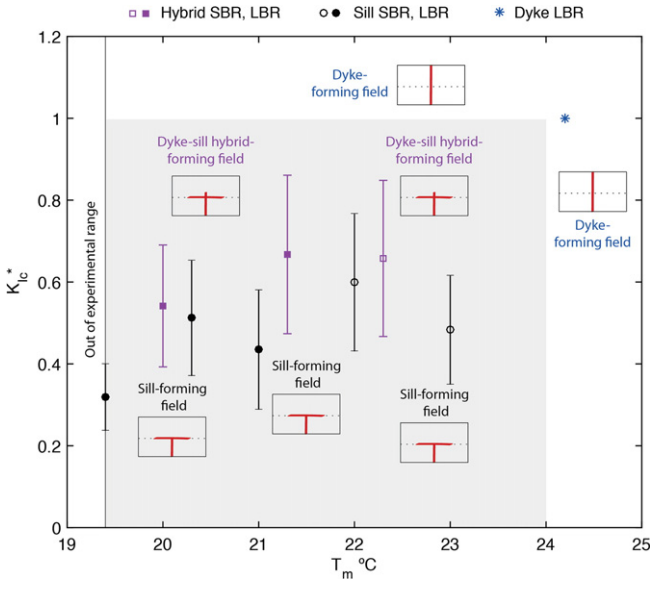

Fig. 10. Experimental intrusion form T_m and K_{Ic}^* (hybrid - purple squares: open SBR, filled LBR; sill - black circles: open SBR, filled LBR, or dyke - blue star: LBR; see Tables 2 and 3 for details). The unshaded region indicates the field of dyke formation where $T_m \geq 19.4$ °C and $K_{Ic}^* \geq 1$, and $T_m > 24$ °C. The shaded region indicates sill-forming and hybrid-forming fields, both occur where $T_m < 24$ °C and $K_{Ic}^* < 1$. Sill formation is associated with relatively low K_{Ic}^* (low K_{IcInt} relative to K_{IcG}). Only experiments with 2.5 wt% concentration gelatine layers are shown, where $E_2 = E_1$. $T_m < 19.4$ °C was not possible experimentally.

$$E' = \frac{E}{1-\nu^2} \tag{9}$$

$$K' = 4K_{Ic}\sqrt{\frac{2}{\pi}} \tag{10}$$

introducing a dimensionless fracture toughness K:

$$K = K'\left(\frac{t^2}{\mu'^5 Q_0^3 E'^{13}}\right)^{1/18}. \tag{11}$$

According to Savitski and Detournay (2002), the viscosity-dominated regime occurs when $K \leq 1$ and toughness-dominated when $K \geq 3.5$.

Applying Savitski and Detournay's (2002) model to study dyke propagation in our experiments we use an estimate of K_{Ic} = 119 Pa m$^{-0.5}$, based on an independent estimate of fracture toughness of a 2.5 wt% gelatine from Kavanagh et al. (2013), to calculate that in our experiments $K > 7$ when $E = 5550$ Pa. Considering sill propagation along an interface, we then calculate sill propagation was in the toughness-dominated regime where $K > 3.5$ even if we assume K_{IcInt} = 16 Pa m$^{-0.5}$ when $E = 5550$ Pa or K_{IcInt} = 23 Pa m$^{-0.5}$ when E = 8880 Pa. Similarly to the equilibrium length and thickness models described in Section 4.2.1, these calculations support our assumption that sill propagation in the experiments was toughness-dominated.

4.4. Boundary conditions: Experiment tank size

Boundary effects were explored by considering the size of tank in which the experiment was carried out. As fluid was intruded into the gelatine to form dykes and sills it displaced the host gelatine, and in the large-tank experiments the amount of displacement due to the dyke intrusion was very small in comparison with the size of the container and so boundary effects were minimal. However, in the small tank experiments this displacement was relatively large and when the sill grew along the interface it very quickly reached the tank wall. We would therefore recommend that the large tank size be the minimum used in future experiments, so that a wider range of experimental variables and intrusion propagation dynamics can be explored.

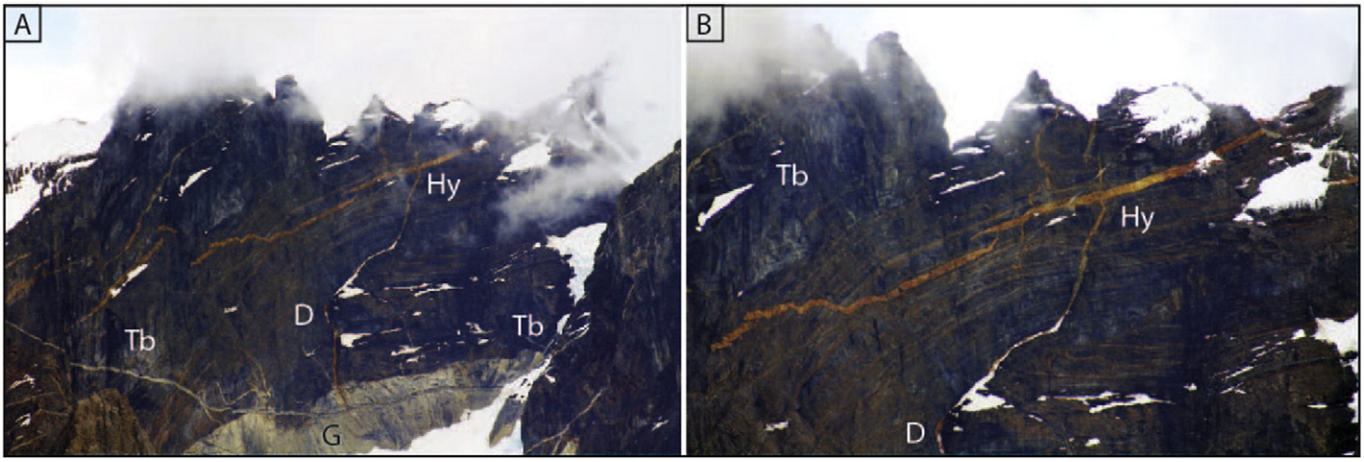

Fig. 12. Photographs of felsic intrusions within a folded turbidite sequence in Las Torres del Paine National Park, Chile. A) Roof contact of a large grey/white granite laccolith (G), where the overlying turbidite sequence (Tb) has been intruded by felsic dykes (D), sills and hybrid (Hy) intrusions that have weathered orange and are approximately 15 m thick. The image shows approximately 600 m of vertical extent. B) Zoomed section of A). The small intrusions are thought to be associated with the growth of the laccolith.

5. Discussion

5.1. The influence of crustal heterogeneity on magma intrusion dynamics

There is good evidence from field observations, geophysical surveys, active monitoring of magma intrusion and numerical models that mechanical layering and rock heterogeneity play an important role in controlling the geometry of magma intrusions in the crust and whether magmas go on to erupt (e.g., Le Corvec et al., 2015; Geshi et al., 2012; Kavanagh et al., 2006; Gudmundsson, 2011; Taisne and Jaupart, 2009). The geometry of the intrusions produced in the gelatine analogue experiments presented here are much simpler than in nature, yet we have produced a range of different intrusion geometries whose form systematically depends on the mechanical properties of the intruded host and especially their contacts. In particular, the importance of the fracture toughness contrast between the intruded layers and their interface, K_{Ic}^*, is identified as a key parameter in determining what type of intrusion forms and how it grows, when the intruded layers are of equal rigidity.

The tendency for magma-filled fractures to utilise rock discontinuities in nature is likely to be variable due to their range of mechanical properties. The Earth's crust is inherently heterogeneous across many scales, comprising mechanically distinct layers that are variably bonded (Kavanagh and Pavier, 2014), and in sub-volcanic areas it has been postulated that most intrusions do not reach the surface (Gudmundsson, 1983). A recent survey of a well-exposed sub-volcanic plumbing system in Utah found that >92% of intrusive material in the field occurred in sill-like bodies (Richardson et al., 2015) that had formed between layers of sandstone and siltstone. In intra-plate settings, the alignment of volcanic vents along pre-existing structures (joints or faults) indicates these have been used to assist magma ascent to eruption (e.g. Le Corvec et al., 2013). Our results suggest that when the fracture toughness of a rock interface is lower than that of the adjacent rocks, sills and dyke-sill hybrids will form rather than dykes that erupt. Mechanical discontinuities and crustal heterogeneity are therefore highly significant in the preferential formation of sills, dyke-sill hybrids and the development of sub-volcanic plumbing systems.

5.2. Dyke-sill hybrids in nature, implications for large magma body growth

Dyke-sill transitions and dyke-sill hybrid structures are only rarely reported in field studies, perhaps due to the lateral extent of sills being very large in comparison to their feeder dyke and so less likely to be exposed. They are also difficult to image in seismic reflection surveys. Despite this, dyke-sill hybrids have been observed in nature in exceptional exposures of intrusive networks in Patagonia. Fig. 12 shows photographs of felsic dyke-sill hybrids and surrounding dykes and sills that have intruded a folded turbidite sequence in the Torres del Paine National Park, Chile. These intrusions are part of the Torres del Paine Intrusive Complex (TPIC) and have intruded rocks that comprise intercalated sandstone, siltstone and mudstone layers. The heterogeneity of the host rock may have played an important role in the development of the intrusive magma structures. The intrusions have protruded from the roof of a large granite laccolith body which has intruded the rock layers below (see bottom of Fig. 11A). The close proximity of the small dyke-sill hybrids with the large igneous body suggests they are associated. This is supported by mapping and geochronology of the TPIC, which indicates that the laccolith was built by incremental growth (e.g. Leuthold et al., 2012) and the accumulation of dykes, sills and hybrid structures within the crust. So-called 'christmas tree' laccolith structures (e.g. Corry, 1988; Rocchi et al., 2010) may have formed in a similar way. Our results suggest that the relative scarcity of hybrid intrusion geometries in nature could be explained by the mechanical conditions that enable their formation being relatively difficult to achieve, requiring rock layers that have similar Young's modulus and similar layer and interface fracture toughness. By better constraining the conditions for dyke, sill and hybrid formation we may also provide insights on the formation and growth of larger magma bodies (Annen et al., 2015).

5.3. Pressure changes during sill and dyke-sill hybrid formation

In a previous study, Kavanagh et al. (2015) demonstrated how strain evolution is correlated with stress changes in experiments where gelatine deforms elastically. Our results support this finding, as the distribution of stress change in the gelatine observed using polarised light (see Fig. 3 and Supplementary Video Fig. 3) is very similar to the pattern of strain evolution quantified using DIC (see Figs. 4 and 5, and Supplementary Video Figs. 4 and 5). The controlled-flux experiments demonstrate that during dyke-sill hybrid growth, fluid extracted from both the feeder dyke in the lower layer and the upper layer dyke protrusion contribute to sill growth. Assuming the fluid is coupled to the gelatine at the dyke margin, stress changes in the gelatine can be related to pressure changes in the fluid. In the experiments, dyke-sill hybrid formation coincided with a decrease in total strain in the gelatine host, and therefore a decrease in fluid pressure within the intrusion as the sill formed (see Figs. 4, 5, 6 and Supplementary Video Figs. 4 and 5). This pressure decrease was documented early in the formation of the hybrid structure, when the influence from the lateral boundary conditions was minimal, and amounted to ~40% reduction in pressure. However, this pressure

reduction is less than has been previously documented in experimental studies of sill formation events (Kavanagh et al., 2015) where >60% pressure reduction has been measured.

In nature, pressure changes in magma can be significant with the potential to destabilise the dyke-sill network if gas exsolution and crystallisation is induced (e.g. Tarasewicz et al., 2012). The dyke-sill hybrid experiment (MOPIV6) had a more rigid upper layer and a lower fracture toughness interface than the sill-forming experiment (see Kavanagh et al., 2015). This mechanical heterogeneity of the host gelatine, the development of a hybrid structure, and the impact of the dyke protrusion in the upper layer may have contributed to smaller pressure fluctuations in the dyke-sill hybrid experiments compared to the sill-forming experiments.

Our results suggest that the mechanical properties of the rock layers and their discontinuities are likely to influence the magnitude of pressure changes experienced by intruding magmas. The mechanical conditions that induce magmatic pressure variations will be of significance for constraining the conditions that may enhance gas exsolution, increase magma ascent rates and therefore potentially lead to volcanism. The mechanical heterogeneity of crustal rock layers and their discontinuities should therefore be considered as a key parameter in models of magma ascent through the crust.

6. Conclusions

Dyke fissures, sills and dyke-sill hybrids were formed in a series of gelatine analogue experiments to study magma ascent through a layered-elastic crust. When the intruded layers were of equal rigidity, we defined K_{Ic}^* as the relative magnitude of fracture toughness of the gelatine layers K_{IcG} and their bonded interface K_{IcInt}. Dyke formation occured when $K_{Ic}^* \geq 1$, whereas dyke-sill hybrids or sills formed when $K_{Ic}^* < 1$. Sill formation was associated with relatively low values of K_{IcInt} and K_{Ic}^*. The mixture temperature T_m of gelatine layer 2 during preparation of the experiment correlates positively with K_{IcInt}, and an upper limit for K_{IcInt} is reached when T_m is 24–25 °C. The photo-elastic properties of gelatine allowed the stress development and evolution to be visualised during the growth of the intrusions, which correlate well with strain evolution in the gelatine host mapped using DIC. Dyke-sill hybrid formation was associated with a significant fluid pressure decrease, though the effect was less than in sill-forming experiments. The experiments highlight the importance of mechanical layering and heterogeneities, such as interface properties, on the geometry and propagation of magmatic intrusions and their tendency to erupt. The relative scarcity of dyke-sill hybrid intrusions in nature could be explained by the conditions required for their formation being unusual or difficult to achieve, and instead the mechanical state of the crust leads to the preferential development of either dykes or sills.

Supplementary data to this article can be found online at http://dx.doi.org/10.1016/j.tecto.2016.12.027.

Acknowledgments

JK acknowledges a Royal Society Research Grant (RG130771). BR and JK thank support from the University of Liverpool. DB and AC thank Monash University for supporting the analogue modelling laboratory. Thierry Menand, Agust Gudmundsson and the editor Rob Govers are thanked for their thoughtful reviews which have helped to improve the manuscript. Andrew Bunger and Dan Faulkner are thanked for helpful discussions. Pete Kokelaar is thanked for comments on a previous version of the manuscript.

References

Adam, J., Urai, J.L., Wieneke, B., Oncken, O., Pfeiffer, K., Kukowski, N., Lohrmann, J., Hoth, S., Van Der Zee, W., Schmatz, J., 2005. Shear localisation and strain distribution during tectonic faulting—new insights from granular-flow experiments and high-resolution optical image correlation techniques. J. Struct. Geol. 27 (2), 283–301.

Anderson, E.M., 1938. The dynamics of sheet intrusion. Proc. R. Soc. Edinb. 58 (3), 242–251.

Annen, C., Blundy, J.D., Sparks, R.S.J., 2006. The genesis of intermediate and silicic magmas in deep crustal hot zones. J. Petrol. 47 (3), 505–539.

Annen, C., Blundy, J.D., Leuthold, J., Sparks, R.S.J., 2015. Construction and evolution of igneous bodies: Towards an integrated perspective of crustal magmatism. Lithos 230, 206–221.

Barnes, S.J., Cruden, A., Arnt, N., Saumur, B., 2016. The mineral system approach applied to magmatic Ni-Cu-PGE sulfide deposits. Ore Geol. Rev. 76, 296–316.

Blundy, J., et al., 2015. Generation of porphyry copper deposits by gas–brine reaction in volcanic arcs. Nat. Geosci. 8 (3), 235–240.

Bunger, A.P., Cruden, A.R., 2011. Modeling the growth of laccoliths and large mafic sills: role of magma body forces. J. Geophys. Res. 116 (B02203). http://dx.doi.org/10.1029/2010JB007648.

Chanceaux, L., Menand, T., 2014. Solidification effects on sill formation: an experimental approach. Earth Planet. Sci. Lett. 403 (C), 79–88.

Chanceaux, L., Menand, T., 2016. The effects of solidification on sill propagation dynamics and morphology. Earth Planet. Sci. Lett. 442, 39–50.

Coleman, D.S., Gray, W., Glazner, A.F., 2004. Rethinking the emplacement and evolution of zoned plutons: geochronologic evidence for incremental assembly of the Tuolumne Intrusive Suite, California. Geology 32 (5), 433–436.

Corry, C.E., 1988. Laccoliths: mechanics of emplacement and growth. Geol. Soc. Am. Spec. Pap. 220.

Crisp, J.A., 1984. Rates of magma emplacement and volcanic output. J. Volcanol. Geotherm. Res. 20, 177–211.

Cruden, A.R., McCaffrey, K.J.W., 2001. Growth of plutons by floor subsidence: implications for rates of emplacement, intrusion spacing and melt-extraction mechanisms. Phys. Chem. Earth A 26 (4–5), 303–315.

Daniels, K.A., Menand, T., 2015. An experimental investigation of dyke injection under regional extensional stress. J. Geophys. Res. 120 (3), 2014–2035.

Delaney, P.T., Pollard, D.D., Ziony, J.I., McKee, E.H., 1986. Field relations between dikes and joints: emplacement processes and paleostress analysis. J. Geophys. Res. Solid Earth 91 (B5), 4920–4938.

Di Giuseppe, E., Funiciello, F., Corbi, F., Ranalli, G., Mojoli, G., 2009. Gelatins as rock analogs: A systematic study of their rheological and physical properties. Tectonophysics 473 (3), 391–403.

Fiske, R.S., Jackson, E.D., 1972. Orientation and growth of Hawaiian volcanic rifts: the effect of regional structure and gravitational stresses. Proc. R. Soc. A Math. Phys. Eng. Sci. 329 (1578), 299–326.

Galland, O., Holohan, E.P., Van Vyk De Vries, B., Burchardt, S., 2015. Laboratory modelling of volcano plumbing systems: a review. Advance in Volcanology. Springer, pp. 1–68.

Gernon, T.M., Field, M., Sparks, R.S.J., 2012. Geology of the Snap Lake kimberlite intrusion, Northwest Territories, Canada: field observations and their interpretation. J. Geol. Soc. 169 (1), 1–16.

Geshi, N., Kusumoto, S., Gudmundsson, A., 2012. Effects of mechanical layering of host rocks on dike growth and arrest. J. Volcanol. Geotherm. Res. 223-224 (C), 74–82.

Glazner, A.F., Bartley, J.M., Coleman, D.S., Gray, W., Taylor, R.Z., 2004. Are plutons assembled over millions of years by amalgamation from small magma chambers? GSA today 14 (4/5), 4–12.

Gudmundsson, A., 1983. Form and dimensions of dykes in eastern Iceland. Tectonophysics 95 (3–4), 295–307.

Gudmundsson, A., 2002. Emplacement and arrest of sheets and dykes in central volcanoes. J. Volcanol. Geotherm. Res. 116, 279–298.

Gudmundsson, A., 2011. Deflection of dykes into sills at discontinuities and magma-chamber formation. Tectonophysics 500 (1–4), 50–64.

Gudmundsson, A., Brenner, S.L., 2005. On the conditions of sheet injections and eruptions in stratovolcanoes. Bull. Volcanol. 67 (8), 768–782.

Gudmundsson, A., Løtveit, I.F., 2014. Sills as fractured hydrocarbon reservoirs: examples and models. Geol. Soc. Lond. Spec. Publ. 374 (1), 251–271.

Hubbert, M.K., 1937. Theory of scale models as applied to the study of geologic structures. Bull. Geol. Soc. Am. 48 (10), 1459–1517.

Hyndman, D.W., Alt, D., 1987. Radial dikes, laccoliths, and gelatin models. J. Geol. 95, 763–774.

Kavanagh, J.L., Pavier, M.J., 2014. Rock interface strength influences fluid-filled fracture propagation pathways in the crust. J. Struct. Geol. 63, 68–75.

Kavanagh, J.L., Sparks, R.S.J., 2011. Insights of dyke emplacement mechanics from detailed 3D dyke thickness datasets. J. Geol. Soc. 168 (4), 965–978.

Kavanagh, J.L., Menand, T., Sparks, R.S.J., 2006. An experimental investigation of sill formation and propagation in layered elastic media. Earth Planet. Sci. Lett. 245 (3–4), 799–813.

Kavanagh, J., Menand, T., Daniels, K.A., 2013. Gelatine as a crustal analogue: Determining elastic properties for modelling magmatic intrusions. Tectonophysics 582, 101–111.

Kavanagh, J.L., Boutelier, D., Cruden, A.R., 2015. The mechanics of sill inception, propagation and growth: Experimental evidence for rapid reduction in magmatic overpressure. Earth Planet. Sci. Lett. 421, 117–128.

Le Corvec, N., Spörli, K.B., Rowland, J., Lindsay, J., 2013. Spatial distribution and alignments of volcanic centers: clues to the formation of monogenetic volcanic fields. Earth Sci. Rev. 124, 96–114.

Le Corvec, N., McGovern, P.J., Grosfils, E.B., 2015. Effects of crustal-scale mechanical layering on magma chamber failure and magma propagation within the Venusian lithosphere. J. Geophys. Res. Planets 120 (7), 1279–1297.

Leuthold, J., Müntener, O., Baumgartner, L.P., Putlitz, B., Ovtcharova, M., Schaltegger, U., 2012. Time resolved construction of a bimodal laccolith (Torres del Paine, Patagonia). Earth Planet. Sci. Lett. 325, 85–92.

Lister, J.R., Kerr, R.C., 1991. Fluid-mechanical models of crack propagation and their application to magma transport in dyke. J. Geophys. Res. 96, 10049–10077.
Loughlin, S.C., Sparks, S., Brown, S.K., Vye-Brown, C., Jenkins, S.F. (Eds.), 2015. Global Volcanic Hazards and Risk. Cambridge University Press, Cambridge, UK.
Magee, C., Jackson, C.A.L., Schofield, N., 2013. The influence of normal fault geometry on igneous sill emplacement and morphology. Geology 41 (4), 407–410.
Malthe-Sørenssen, A., Planke, S., Svensen, H., Jamtveit, B., 2004. Formation of saucer-shaped sills. Physical Geology of High-Level Magmatic Systems. Geol. Soc. Lond. Spec. Publ. 234, 215–227.
Menand, T., Tait, S.R., 2002. The propagation of a buoyant liquid-filled fissure from a source under constant pressure: an experimental approach. J. Geophys. Res. 107 (2306), 177–185.
Muirhead, J.D., Airoldi, G., White, J.D., Rowland, J.V., 2014. Cracking the lid: Sill-fed dikes are the likely feeders of flood basalt eruptions. Earth Planet. Sci. Lett. 406, 187–197.
Naldrett, A.J., 2011. Fundamentals of magmatic sulfide deposits. Rev. Econ. Geol. 17, 1–50.
Pollard, D.D., Johnson, A.M., 1973. Mechanics of growth of some laccolithic intrusions in the Henry mountains, Utah, II: bending and failure of overburden layers and sill formation. Tectonophysics 18 (3–4), 311–354.
Richardson, J.A., Connor, C.B., Wetmore, P.H., Connor, L.J., Gallant, E.A., 2015. Role of sills in the development of volcanic fields: Insights from lidar mapping surveys of the San Rafael Swell, Utah. Geology 43 (11), 1023–1026.
Rivalta, E., Böttinger, M., Dahm, T., 2005. Buoyancy-driven fracture ascent: experiments in layered gelatine. J. Volcanol. Geotherm. Res. 144 (1–4), 273–285.
Rivalta, E., et al., 2015. A review of mechanical models of dike propagation: schools of thought, results and future directions. Tectonophysics 638, 1–42.
Rocchi, S., Westerman, D.S., Dini, A., Farina, F., 2010. Intrusive sheets and sheeted intrusions at Elba Island, Italy. Geosphere 6 (3), 225–236.
Savitski, A.A., Detournay, E., 2002. Propagation of a penny-shaped fluid-driven fracture in an impermeable rock: asymptotic solutions. Int. J. Solids Struct. 39, 6311–6337.
Schrank, C.E., Boutelier, D.A., Cruden, A.R., 2008. The analogue shear zone: from rheology to associated geometry. J. Struct. Geol. 30 (2), 177–193.
Sigmundsson, F., Hreinsdóttir, S., Hooper, A., Árnadóttir, T., Pedersen, R., Roberts, M.J., Óskarsson, N., Auriac, A., Decriem, J., Einarsson, P., Geirsson, H., 2010. Intrusion triggering of the 2010 Eyjafjallajokull explosive eruption. Nature 468 (7322), 426–430.
Taisne, B., Jaupart, C., 2009. Dike propagation through layered rocks. J. Geophys. Res. Solid Earth 114 (B9). http://dx.doi.org/10.1029/2008JB006228.
Taisne, B., Tait, S., 2009. Eruption versus intrusion? Arrest of propagation of constant volume, buoyant, liquid-filled cracks in an elastic, brittle host. J. Geophys. Res. 114 (B6), B06202.
Taisne, B., Tait, S., 2011. Effect of solidification on a propagating dike. J. Geophys. Res. 116 (B1), B01206.
Takada, A., 1989. Magma transport and reservoir formation by a system of propagating cracks. Bull. Volcanol. 52, 118–126.
Takada, A., 1990. Experimental study on propagation of liquid-filled crack in gelatin: shape and velocity in hydrostatic stress condition. J. Geophys. Res. 95, 8471–8481.
Tarasewicz, J., Brandsdóttir, B., White, R.S., Hensch, M., Thorbjarnardóttir, B., 2012. Using microearthquakes to track repeated magma intrusions beneath the Eyjafjallajökull stratovolcano, Iceland. J. Geophys. Res. Solid Earth 117 (B00C06). http://dx.doi.org/10.1029/2011JB008751.
van Otterloo, J., Cruden, A.R., 2016. Rheology of pig skin gelatine: defining the elastic domain and its thermal and mechanical properties for geological analogue experiment applications. Tectonophysics 683, 86–97.
White, J.L., et al., 2012. Kimberlite sills and dykes associated with the Wesselton Kimberlite Pipe, Kimberley, South Africa. S. Afr. J. Geol. 115 (1), 1–32.